Mechanics Research Communications 103 (2020) 103460

Contents lists available at ScienceDirect

Mechanics Research Communications

journal homepage: www.elsevier.com/locate/mechrescom

An exact approach to the dynamics of locally-resonant beams

Giuseppe Failla [a,*], Roberta Santoro [b], Andrea Burlon [a], Andrea Francesco Russillo [a]

[a] Department of Civil, Environmental, Energy and Materials Engineering (DICEAM), University of Reggio Calabria, Via Graziella, 89124 Reggio Calabria, Italy

[b] Department of Engineering, University of Messina, Italy

ARTICLE INFO

Article history:
Received 20 June 2019
Revised 22 October 2019
Accepted 21 November 2019
Available online 29 November 2019

Keywords:
Locally-resonant beam
Resonator
Transmittance
Frequency response
Modal response

ABSTRACT

This paper presents an exact analytical approach to calculate the dynamic response of elastic beams with periodically-attached resonators, generally referred to as locally-resonant beams. Showing that a typical resonator is equivalent to an external constraint, whose reaction force on the beam depends on the deflection of the application point through a pertinent frequency-dependent stiffness, the beam-resonators coupled system is handled using only the beam motion equation, with Dirac's deltas modelling the shear-force discontinuities associated with the reaction forces of the resonators. This is the basis to tackle the dynamics of infinite as well as finite beams, the first by a transfer matrix method to calculate frequency band gaps, the second by a generalized function approach. The dynamics of the finite beam is studied in frequency and time domains deriving the exact frequency response and the exact modal response, including modal frequency and impulse response functions. The proposed approach is formulated for arbitrary number of resonators and loads, and applies for both non-proportional and proportional damping.

1. Introduction

Beams with periodically-attached resonators are an emerging and challenging concept for vibration attenuation, with several potential applications in mechanical and structural engineering [1–10]. Typically, they are modelled as a continuous-discrete system, where resonators are single- or multi-degree-of-freedom mass-spring subsystems coupled with a continuous Euler or Timoshenko beam. The continuous-discrete model has been applied to sandwich beams with embedded resonators [2], hollow aluminium beams with an array of rubber-ring coated copper columns [3], beams carrying beam-like resonators [4], elastic metamaterial beams [5–10]. Beams with periodically-attached resonators are referred to as locally-resonant (LR) beams [1]. Remarkably, the resonators provide elastic wave attenuation over low-frequency ranges named band gaps [1–10], whose number is equal to the resonator degrees of freedom (DOFs). Translational DOFs are generally considered for resonators [1–10], to be activated by the beam displacement at the application point.

Most frequently, solutions for LR beams have been sought in the frequency domain using the spectral element method [3–4], the transfer matrix method [11] and the finite element method [12]. Also, homogenization techniques defining an equivalent mass per unit length [2] or the Galerkin technique in presence of nonlinearity [9] have been used.

The present study aims to introduce a comprehensive framework to calculate frequency and time responses of elastic LR beams. The key is to show that the mass-spring subsystem modeling a resonator can be reverted to an equivalent constraint with reaction force depending on the deflection of the application point through a suitable frequency-dependent stiffness. Indeed, a pertinent stiffness will be derived for single- or multi-degree-of-freedom resonators generally considered in the literature [1–10]. Starting from this basis, a transfer matrix method will be adopted to calculate band gaps of the infinite beam, while the exact frequency and time responses of a finite beam subjected to arbitrary loads will be obtained, in closed analytical form, extending an approach recently introduced by some of the authors [13–15] using the theory of generalized functions [13–20].

The paper is organized as follows. Section 2 derives the frequency-dependent stiffness of typical resonators and formulates the transfer matrix method for infinite beams. Frequency and time domain solutions for finite beams are presented in Section 3. A numerical application is discussed in Section 4. Finally, one Appendix is included.

* Corresponding author.
E-mail address: giuseppe.failla@unirc.it (G. Failla).

https://doi.org/10.1016/j.mechrescom.2019.103460

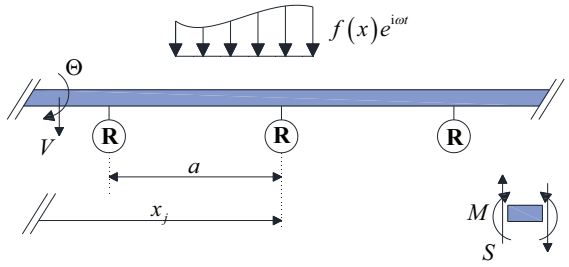

Fig. 1. Elastic LR beam.

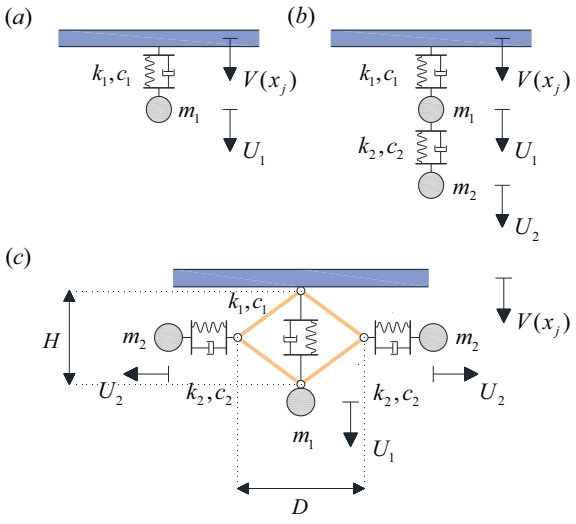

Fig. 2. Examples of resonators: (a) 1-DOF; (b) 2-DOF; (c) laterally-resonant 2-DOF.

2. Local resonance via transfer matrix approach

Fig. 1 shows the simple model of a LR Euler beam. Local resonators are periodically attached to the beam at mutual distance a (= cell length). Symbol "R" denotes a resonator, typically with single or multiple DOFs as shown in Fig. 2.

In the frequency domain, the reaction force of resonators in Fig. 2 can be expressed in terms of the deflection of the application point by using the resonator motion equations. For instance, the motion equations of the 2-DOF resonator in Fig. 2c are [10]:

$$m_2\omega^2 U_2 - \eta_2(\omega)[U_2 + \lambda(U_1 - V)/2] = 0 \tag{1a}$$

$$m_1\omega^2 U_1 - \eta_1(\omega)(U_1 - V) - \lambda\eta_2(\omega)[U_2 + \lambda(U_1 - V)/2] = 0 \tag{1b}$$

where $V = V(x_j)$, $\lambda = H/D$ and $\eta_l(\omega) = k_l + i\omega c_l$, for l = 1,2. From Eqs. (1), the displacements U_1, U_2 and the reaction force of the resonator take the form:

$$U_1 = \frac{H^2\eta_2(\omega)m_2\omega^2 - 2D^2\eta_1(\omega)\left(\eta_2(\omega) - m_2\omega^2\right)}{H^2\eta_2(\omega)m_2\omega^2 - 2D^2\left(\eta_1(\omega) - m_1\omega^2\right)\left(\eta_2(\omega) - m_2\omega^2\right)}V \tag{2}$$

$$U_2 = \frac{DH\eta_2(\omega)m_1\omega^2}{H^2\eta_2(\omega)m_2\omega^2 - 2D^2\left(\eta_1(\omega) - m_1\omega^2\right)\left(\eta_2(\omega) - m_2\omega^2\right)}V \tag{3}$$

$$R(\omega) = -\kappa(\omega)V \tag{4}$$

where $\kappa(\omega)$ is the frequency-dependent stiffness

$$\kappa(\omega) = \frac{m_1\omega^2\left[2D^2\eta_1(\omega)\left(\eta_2(\omega) - m_2\omega^2\right) - H^2m_2\omega^2\eta_2(\omega)\right]}{H^2m_2\omega^2\eta_2(\omega) - 2D^2\left(\eta_1(\omega) - m_1\omega^2\right)\left(\eta_2(\omega) - m_2\omega^2\right)} \tag{5}$$

Likewise, the reaction force of the 2-DOF resonator in Fig. 2b is given as Eq. (4), being

$$\eta_2(\omega)(U_1 - U_2) + m_2\omega^2 U_2 = 0 \tag{6a}$$

$$\eta_2(\omega)(U_2 - U_1) - \eta_1(\omega)(U_1 - V) + m_1\omega^2 U_1 = 0 \tag{6b}$$

$$\kappa(\omega) = \frac{\eta_1(\omega)\left[\eta_2(\omega)(m_1 + m_2)\omega^2 - m_1m_2\omega^4\right]}{\eta_2^2(\omega) - \left(\eta_1(\omega) + \eta_2(\omega) - m_1\omega^2\right)\left(\eta_2(\omega) - m_2\omega^2\right)} \tag{7}$$

Next, consider the nth cell of the LR beam shown in Fig. 1. Being EI the flexural stiffness and ρ the mass density per unit length, for a given frequency ω the motion equation within the nth cell reads (ω-dependence is omitted for brevity)

$$EI\frac{\bar{d}^4V(x)}{dx^4} - \rho\omega^2V(x) = 0 \tag{8}$$

where $V(x)$ is the deflection

$$V(x) = A_n\cos\left(\alpha x'\right) + B_n\sin\left(\alpha x'\right) + C_n\cosh\left(\alpha x'\right) + D_n\sinh\left(\alpha x'\right) \tag{9}$$

for $x' = x$–$(n-1)$a and $\alpha^4 = \rho\omega^2/EI$. Now, enforcing appropriate matching conditions for deflection, rotation, bending moment and shear force at the connection point between nth and $(n-1)$th cells leads to the following equation [21]

$$\boldsymbol{\Psi}_n = \mathbf{T}\boldsymbol{\Psi}_{n-1} = \mathbf{K}^{-1}\mathbf{H}\boldsymbol{\Psi}_{n-1} \tag{10}$$

where $\mathbf{T} = \boldsymbol{K}^{-1}\mathbf{H}$ is the transfer matrix,

$$\mathbf{K} = \begin{bmatrix} 1 & 0 & 1 & 0 \\ 0 & 1 & 0 & 1 \\ -1 & 0 & 1 & 0 \\ F & -1 & F & 1 \end{bmatrix} \tag{11}$$

$$\mathbf{H} = \begin{bmatrix} \cos(\alpha a) & sin(\alpha a) & \cosh(\alpha a) & \sinh(\alpha a) \\ -sin(\alpha a) & \cos(\alpha a) & \sinh(\alpha a) & \cosh(\alpha a) \\ -\cos(\alpha a) & -sin(\alpha a) & \cosh(\alpha a) & \sinh(\alpha a) \\ sin(\alpha a) & -\cos(\alpha a) & \sinh(\alpha a) & \cosh(\alpha a) \end{bmatrix} \tag{12}$$

$$F = \kappa(\omega)\left(\alpha^3 EI\right)^{-1} \tag{13}$$

Now, to investigate wave propagation in an infinite periodic LR beam, assume no damping in every resonator. According to the Bloch theorem [21], it is known that $\boldsymbol{\Psi}_n = e^{iqa}\boldsymbol{\Psi}_{n-1}$, where q is the wave vector in x direction and i = imaginary unit. Combining $\boldsymbol{\Psi}_n = e^{iqa}\boldsymbol{\Psi}_{n-1}$ and Eq. (10) leads to the following standard eigenvalue problem of the transfer matrix $\mathbf{T}$:

$$\det\left(\mathbf{T} - e^{iqa}\mathbf{I}\right) = 0 \tag{14}$$

where $\mathbf{I}$ is the 4 × 4 unit matrix. Eq. (14) gives the values of q for specified ω: if q is real the corresponding wave propagates through the beam, i.e. the frequency ranges associated with real q are pass bands. On the contrary, there is a band gap over a specific frequency range for which no real q exists and, in this case, the imaginary part of q indicates the wave attenuation through one cell of the beam. For convenience, roots of the characteristic Eq. (14) will be sought setting $\gamma = iqa$.

Regarding a finite LR beam, it is known that its frequency band gaps are described effectively by the frequency response function (FRF) [22]. Therefore, the remainder of the paper will derive the exact FRF for a LR finite beam and, in addition, the exact modal response in frequency and time domains.

3. Dynamics of LR finite beam

Assume that the LR beam in Fig. 1 is finite. The vibration response can be represented in the general form

$$\mathbf{y}(x,t)=\mathbf{Y}e^{i\omega t};\ \mathbf{u}_j(t)=\mathbf{U}_j e^{i\omega t} \tag{15}$$

where $\boldsymbol{y}=\{v\ \theta\ m\ s\}^T$, $\boldsymbol{Y}=\{V\ \Theta\ M\ S\}^T$, $\mathbf{u}_j=\{u_j^{(1)}\ u_j^{(2)}\ldots u_j^{(Q)}\}^T$ and $\mathbf{U}_j=\{U_j^{(1)}\ U_j^{(2)}\ldots U_j^{(Q)}\}^T$ collect the response variables of the beam and the Q-DOF resonator applied at $x=x_j$ (e.g., $U_j^{(1)}$=U_1, $U_j^{(2)}$=U_2 in Fig. 2). Eq. (15) will be used as general form to represent:

(a) FRF under an harmonic load with frequency ω, i.e. $\boldsymbol{Y}=\boldsymbol{Y}(x,\omega)$ and $\mathbf{U}_j=\mathbf{U}_j(\omega)$;
(b) free-vibration response, being ω=ω_k an eigenvalue and $\boldsymbol{Y}=\mathbf{Y}_k(x)$, $\boldsymbol{U}=\mathbf{U}_{j,k}$ the corresponding eigenfunctions. Eigenvalues and eigenfunctions may be either real or complex depending on damping in the system.

Since Eq. (4) provides the resonator reaction force in terms of the deflection $V(x_j)$, the response of the beam-resonators coupled system can be obtained from the motion equation of the beam only, generalizing the approach recently proposed by some of the authors in frequency and time domains [13–14].

3.1. Exact frequency response

Be the beam in Fig. 1 subjected to a harmonic load $f(x)e^{i\omega t}$, so that the FRF takes the form (15). The motion equation reads

$$EI\frac{\bar{\mathrm{d}}^4V(x)}{\mathrm{d}x^4}-\sum_{j=1}^{N}R_j\delta\left(x-x_j\right)-\rho\omega^2V(x)=f(x) \tag{16}$$

where bar means generalized derivative, symbol $\delta(x-x_j)$ denotes a Dirac's delta at $x=x_j$, R_j is the reaction force of the j^{th} resonator, i.e. (see Eq. (4))

$$R_j=-\kappa_j(\omega)V\left(x_j\right)\quad j=1,2\ldots N \tag{17}$$

for N = number of resonators. Following ref. [13], it can be written that

$$\mathbf{Y}(x,\omega)=\mathbf{W}(x,\omega)\mathbf{d}+\mathbf{Y}^{(f)}(x,\omega) \tag{18}$$

where $\boldsymbol{d}=\{d_1\ d_2\ d_3\ d_4\}^T$ is a vector of integration constants, $\mathbf{W}(x,\omega)$ is a 4×4 matrix depending on the solution to the homogeneous equation associated with Eq. (16), while $\mathbf{Y}^f(x,\omega)$ is a 4×1 load-dependent vector. Elements in $\mathbf{W}$ and $\mathbf{Y}^f$ are available in an exact analytical form, see Appendix A.

Vector $\mathbf{d}$ in Eq. (18) is obtained enforcing the beam B.C., i.e.

$$\mathbf{Bd}=\mathbf{r}\rightarrow\mathbf{d}=\mathbf{B}^{-1}\mathbf{r} \tag{19}$$

where $\mathbf{B}$ and $\mathbf{r}$ are a 4×4 matrix and a 4×1 vector, built from $\mathbf{W}$ and $\mathbf{Y}^f$ computed at $x=0$ and $x=L$.

The inverse matrix $\boldsymbol{B}^{-1}$ is available in a closed analytical form, as shown in ref. [15]. Hence, replacing Eq. (19) for $\mathbf{d}$ in Eq. (18) provides a closed analytical expression for the FRF $\mathbf{Y}(x,\omega)$ of the beam in Fig. 1. Remarkably, Eq. (18) for $\mathbf{Y}(x,\omega)$ holds for any number of resonators along the beam. The frequency response $\mathbf{U}_j(\omega)$ in the jth resonator can be obtained from the deflection $V(x_j)$ of the application point, e.g. using Eqs. (2)–(3) for the resonator in Fig. 2c.

Eq. (18) holds for homogeneous B.C. Non-homogeneous B.C. associated with resonators applied at the beam end can be still treated as homogeneous, considering an end resonator as an internal resonator located at $x=0^+$ or $x=L^-$.

It is noteworthy that Eq. (18) can be applied to calculate also the transmittance of the beam, which is typically used to assess effectiveness of band gaps in a LR finite beam [8,21]. For this, the reaction force of every resonator shall be set equal to

$$R_j=-\kappa_j(\omega)\left(V\left(x_j\right)+U_g\right) \tag{20}$$

where U_g is the displacement of the ground, while the B.C. are

$$V(0)=0\quad V'(0)=0\qquad V''(0)=0\quad V'''(0)=0 \tag{21a-d}$$

being $V(x)$ the deflection relative to the ground.

3.2. Exact modal response

Next, be the beam in Fig. 1 subjected to an impulsive loading $f(x)\delta(t)$, where $\delta(t)$ is a Dirac's delta in time and $f(x)$ a space-dependent function. Adopting the approach in ref. [13], the impulse response function (IRF) $\mathbf{h}(x,t)=\{h_v\ h_\theta\ h_m\ h_s\}^T$ of the beam can be represented by modal superposition as

$$\mathbf{h}(x,t)=\sum_{k=1}^{\infty}\mathbf{h}_k(x,t)=\sum_{k=1}^{\infty}g_k(t)\mathbf{Y}_k(x) \tag{22}$$

$$g_k(t)=\hat{g}_k e^{i\omega_k t}k=1,2\ldots \tag{23}$$

being $\hat{g}_k$ a complex coefficient, while ω_k and $\mathbf{Y}_k(x)$ are eigenvalue and vector of eigenfunctions associated with the kth mode. Namely, ω_k and $\mathbf{Y}_k$ are complex if damping is not proportional, real if damping is proportional. The eigenvalue problem is $\mathbf{B}(\omega)\mathbf{d}=\mathbf{0}$, i.e. Eq. (19) with $\mathbf{r}$=$\mathbf{0}$.

Based on ref. [13], $\hat{g}_k$ can be obtained as

$$\hat{g}_k=\chi_k(i\omega_k\Pi_k)^{-1} \tag{24}$$

$$\chi_k=\int_0^L f(x)V_k(x)\mathrm{d}x \tag{25}$$

$$\Pi_k=\sum_{j=1}^{N}\sum_{l=1}^{4}\mu_j(\omega_k)V_k^2\left(x_j\right)+2\rho\int_0^L V_k^2(x)dx \tag{26}$$

Terms in Eq. (26) depend on the type of resonator. Specifically, $\mu_j(\omega_k)$ is obtained from the following limit that involves the frequency-dependent stiffness of the resonator

$$\lim_{\omega_n\rightarrow\omega_k}\frac{\omega_n\left(\kappa_j(\omega_n)-\kappa_j(\omega_k)\right)}{(\omega_k-\omega_n)}=\omega_k^2\mu_j(\omega_k) \tag{27}$$

For instance, for the resonator in Fig. 2c

$$\mu_j(\omega_k)=\frac{2m_1}{g(\omega_k)}\sum_{s=1}^{3}f_s(\omega_k) \tag{28}$$

$$\begin{aligned}f_1&=H^4m_2^2\omega_n^4\eta_2^2(\omega_n)+2D^4\left(2k_1^2+4i\omega_nc_1k_1-c_1\omega_n^2(2c_1+i\omega_nm_1)\right)\\&\quad\times\left(\eta_2(\omega_n)-m_2\omega_n^2\right)^2\\f_2&=D^2H^2m_2\omega_n^2\left[-4k_1\eta_2(\omega_n)\left(\eta_2(\omega_n)-m_2\omega_n^2\right)\right.\\&\quad\left.+4c_1\left(c_2\omega_n^2-ik_2\omega_n\right)\left(\eta_2(\omega_n)-m_2\omega_n^2\right)\right]\\f_3&=D^2H^2m_1m_2\omega_n^4\left[2k_2^2+4i\omega_nc_2k_2-c_2\omega_n^2(2c_2+i\omega_nm_2)\right]\\g&=\left\{2D^2\left[\left(\eta_1(\omega_n)-m_1\omega_n^2\right)\left(\eta_2(\omega_n)-m_2\omega_n^2\right)\right]\right.\\&\quad\left.-H^2m_2\omega_n^2\eta_2(\omega_n)\right\}^2\end{aligned} \tag{29}$$

Now it is known that, for typical damping levels in engineering applications, modes contributing to the beam response occur in complex conjugate pairs, i.e. $g_k(t)$ in Eq. (23) may be $\hat{g}_ke^{i\omega}k^t$ as well as $\hat{g}_k{}^*e^{-i\omega}k^t$, with $\hat{g}_k{}^*$ complex conjugate of $\hat{g}_k$. The result is the following real form of the modal IRFs for the kth mode in Eq. (22):

$$\mathbf{h}_k(x,t)=\boldsymbol{\varphi}_k(x)|\omega_k|z_k(t)+\boldsymbol{\psi}_k(x)\dot{z}_k(t) \tag{30}$$

where

$$\boldsymbol{\varphi}_k(x)=\zeta_k\boldsymbol{\psi}_k(x)-\sqrt{1-\zeta_k^2}\boldsymbol{\lambda}_k(x) \tag{31}$$

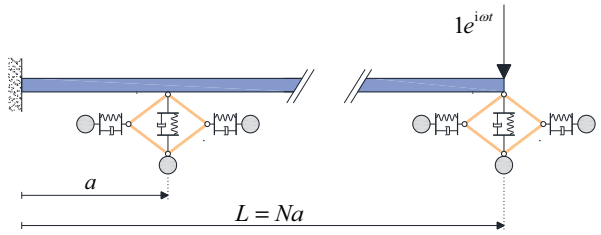

Fig. 3. Elastic LR beam with resonators in Fig. 2c.

$$\boldsymbol{\psi}_k(x) = 2\mathrm{Re}\left[\hat{g}_k \mathbf{Y}_k(x)\right]; \boldsymbol{\lambda}_k(x) = 2\mathrm{Im}\left[\hat{g}_k \mathbf{Y}_k(x)\right] \tag{32a.b}$$

$$z_k(t) = \frac{1}{\omega_{Dk}} e^{-\zeta_k|\omega_k|t} \sin(\omega_{Dk}t); \omega_{Dk} = |\omega_k|\sqrt{1-\zeta_k^2} \tag{33a.b}$$

being $\zeta_k = \mathrm{Im}[\omega_k]/|\omega_k|$ the modal damping ratio. Finally, the modal FRF $\boldsymbol{H}_k = \{H_{v,k}\ H_{\theta,k}\ H_{m,k}\ H_{s,k}\}^T$ of the beam is [13]

$$\mathbf{H}_k(x,\omega) = \boldsymbol{\varphi}_k(x)|\omega_k|H_k(\omega) + \boldsymbol{\psi}_k(x)\mathrm{i}\omega H_k(\omega) \tag{34}$$

$$H_k(\omega) = \frac{1}{|\omega_k|^2 - \omega^2 + \mathrm{i}2\zeta_k|\omega_k|\omega} \tag{35}$$

Eq. (34) approximates the exact FRF (18) providing an insight into the single modal contributions, i.e.

$$\mathbf{Y}(x,\omega) \approx \sum_{k=1}^{M} \mathbf{H}_k(x,\omega) \tag{36}$$

where M is the number of modes retained for practical purpose. The IRF and FRF in every resonator follow from Eq. (22) and Eq. (36), provided that $\mathbf{Y}_k$ is replaced with $\mathbf{U}_{j,k}$, i.e. the vector of eigenfunctions associated with the kth mode for the response in the jth resonator. Specifically, $\mathbf{U}_{j,k}$ can be calculated from the deflection $V_k(x_j)$ of the application point (e.g. using Eqs. (2)–(3) for the resonator in Fig. 2c).

Eq. (22) for IRF and Eq. (36) and FRF hold for any number of resonators along the beam. Every modal contribution (30) and (34) is exact and readily obtainable in analytical form once the eigenvalues are calculated. For practical purposes, a sufficient number of modes M shall be retained in Eq. (22) and Eq. (36) to obtain accurate expressions for IRF and FRF.

Finally, it is noteworthy that Eq. (22) for IRF and Eq. (36) for the FRF hold a similar form also for proportional damping [15]

$$\mathbf{h}_k(x,t) = \frac{2\chi_k}{\omega_{Dk}\Pi_k} e^{-\zeta_k\omega_k t} sin(\omega_{Dk}t)\mathbf{Y}_k(x) \tag{37}$$

$$\mathbf{H}_k(x,\omega) = \frac{2\chi_k}{\Pi_k} H_k(\omega)\mathbf{Y}_k(x) \tag{38}$$

where ζ_k is the modal damping ratio, ω_{Dk} is given by Eq. (33b) and $H_k(\omega)$ by Eq. (35) on replacing $|\omega_k|$ with the real frequency ω_k of the kth mode.

4. Numerical application

4.1. Example A

Consider the cantilever aluminium beam in Fig. 3 carrying the laterally-resonant 2-DOF resonators in Fig. 2c [10]. Parameters are: $E = 70$ GPa, $I = 7.85 \times 10^{-9}$ m^4 (corresponding to a circular cross section of radius $= 0.01$ m), $\rho = 0.88$ kg m^{-1}, $N = 8$, $a = 0.02$ m, $H = D = 0.01$ m, $m_1 = 0.01$ kg, $m_2 = 0.005$ kg, $k_1 = k_2 = 10^5$ Nm^{-1}, $c_1 = c_2 = 0.1$ Nsm^{-1} (see Fig. 2c). The beam

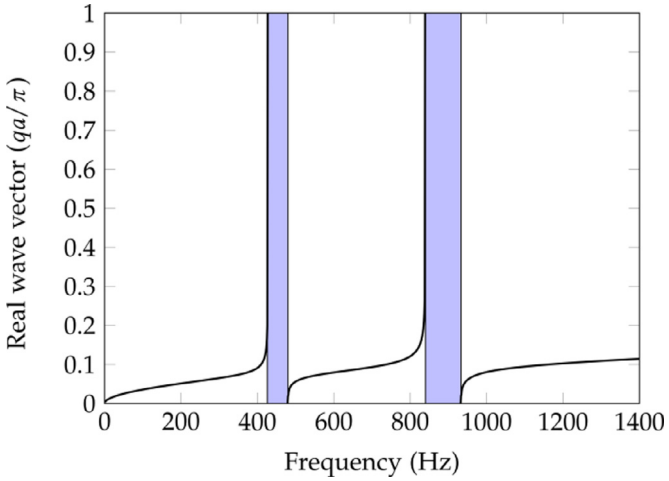

Fig. 4. Band gaps of the LR beam in Fig. 3.

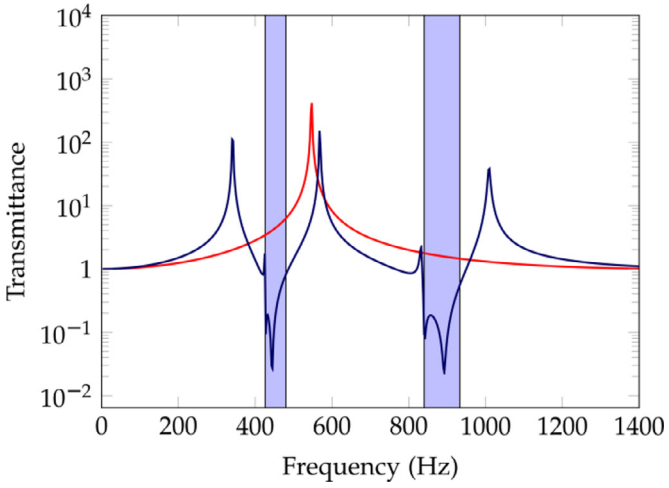

Fig. 5. Transmittance of the beam in Fig. 3: with resonators (blue) and without resonators (red). (For interpretation of the references to colour in this figure legend, the reader is referred to the web version of this article.)

may be thought of as the elastic support for a machinery/structure exerting transverse loads.

In order to have a preliminary insight into the elastic wave attenuation properties, the band gaps of the infinite beam with no damping are calculated using Eq. (14). Fig. 4 shows that two band gaps exist in the frequency ranges 426–480 Hz and 840–933 Hz, where no real wave vectors are found.

Next, Fig. 5 shows the transmittance of the cantilever beam in Fig. 3. It is noticed that the wave attenuation properties of the infinite beam hold also for the finite beam, as indeed the transmittance within the band gaps is lower than that over the remaining frequency domain by more than one order of magnitude. Notice that the transmittance is equal to 1 for zero frequency, as expected for a static unit ground displacement. For comparison, Fig. 5 shows the transmittance of the beam without resonators, which exhibits a single peak but larger than the peaks of the beam with resonators.

For a further insight into the dynamics of the beam in Fig. 3. Fig. 6 shows the FRF for the tip deflection under a unit harmonic force applied at the free end, obtained by the exact Eq. (18) and the approximate Eq. (36) using $M = 7$ modes (pertinent complex eigenvalues are in Table 1). The modal FRFs (34) are also reported in Fig. 6 to highlight the contribution of every mode.

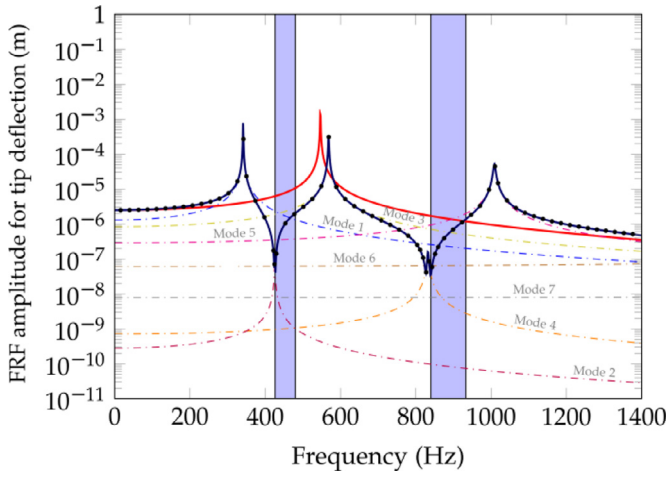

Fig. 6. FRF for the tip deflection of the beam in Fig. 3, under a unit harmonic force applied at the free end: Eq. (18) (blue); Eq. (36) with $M = 7$ modes (black dots); Eq. (34) for modal FRFs (color dashes); beam without resonators (red). (For interpretation of the references to colour in this figure legend, the reader is referred to the web version of this article.)

Table 1
Eigenvalues and damping ratios for modes of beam in Fig. 3.

Mode	Eigenvalue	Damping ratio
1	± 2143.994 + 1.076253i	0.000502
2	± 2672.508 + 3.545824i	0.001326
3	± 3570.584 + 4.171392i	0.001168
4	± 5229.014 + 13.43045i	0.002568
5	± 6338.494 + 17.59552i	0.002776
6	± 21,786.56 + 6.095178i	0.000279
7	± 60,345.95 + 5.750229i	0.000095

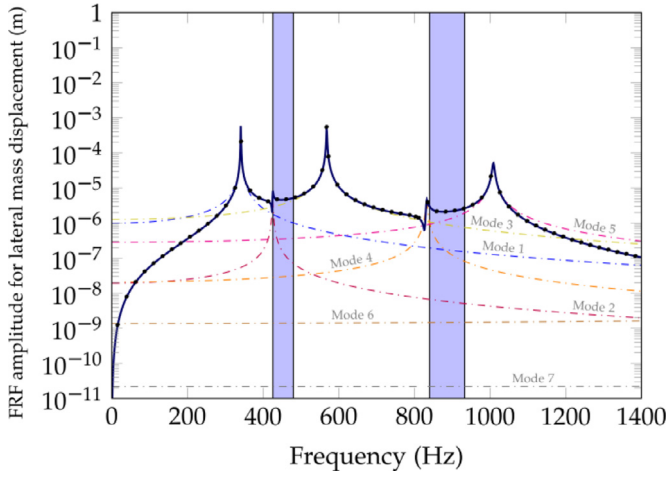

Fig. 7. FRF for the displacement of the lateral mass within the resonator at the free end of the beam in Fig. 3, under a unit harmonic force applied at the free end: Eq. (18) (blue); Eq. (36) with $M = 7$ modes (black dots); Eq. (34) for modal FRFs (color dashes). (For interpretation of the references to colour in this figure legend, the reader is referred to the web version of this article.)

Further, Fig. 7 shows the FRF for the displacement of the lateral masses within the resonator placed at the free end. Interestingly, the peak values of the FRF are all outside the band gaps. This is evidence that the resonators ensure wave attenuation properties vibrating within a limited displacement range, which is obviously desirable for a consistent design of the LR beam.

Next, consider again Fig. 6. It is noticed that the FRF, within the band gaps, is generally well lower than the corresponding one of the beam without resonators. The only exception is at the right

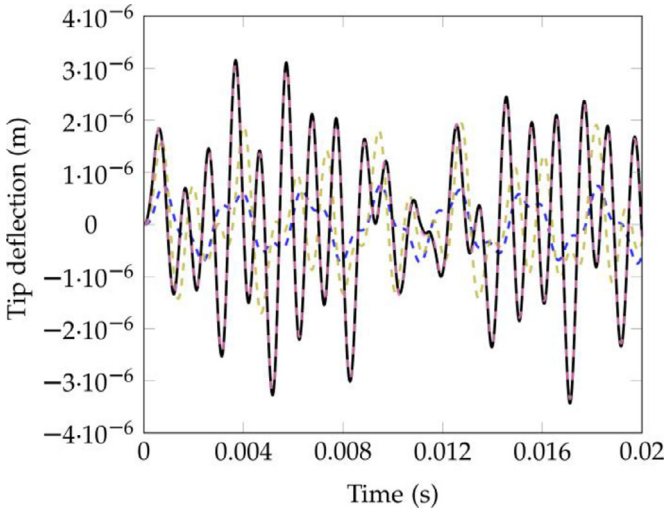

Fig. 8. Time response for the tip deflection of the beam in Fig. 3 under a 920-Hz unit sine force at the free end, for increasing number of modes M in Eq. (22): $M = 1$ (blue dashes), $M = 3$ (yellow dashes), $M = 5$ (pink dashes) $M = 7$ (black). (For interpretation of the references to colour in this figure legend, the reader is referred to the web version of this article.)

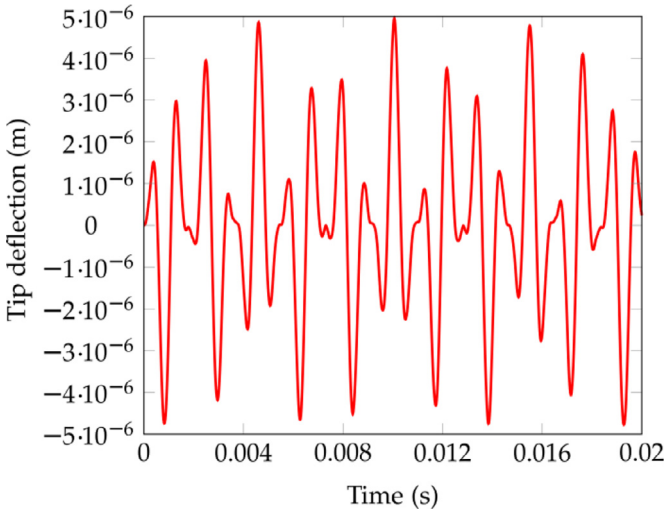

Fig. 9. Time response for the tip deflection of the beam in Fig. 3 without resonators, under a 920-Hz unit sine force at the free end.

end of the second band gap, where the FRFs of the beam with and without resonators are very close to each other. This behaviour is essentially attributable to the 3rd and 5th modes, whose modal FRFs are significant within that frequency range (see pink and yellow lines in Fig. 6).

To further investigate this issue, Figs. 8 and 9 report the time responses for tip deflection under a 920-Hz unit sine force applied at the tip, for the beam in Fig. 3 with and without resonators (920 Hz is chosen as a forcing frequency close to the right end of the second band gap in Fig. 6). Consistently with the results in Fig. 7, it is found that the beam response is mainly dominated by 3rd and 5th modal contributions and, due to these modes, the responses of the beam with resonators (black line in Fig. 8) and without resonators (Fig. 9) have almost the same order of magnitude. This is a crucial information for design purposes because, e.g., once mass and stiffness of the resonators are calibrated, damping coefficients might be selected so as to minimize the contribution of the 3rd and 5th modes.

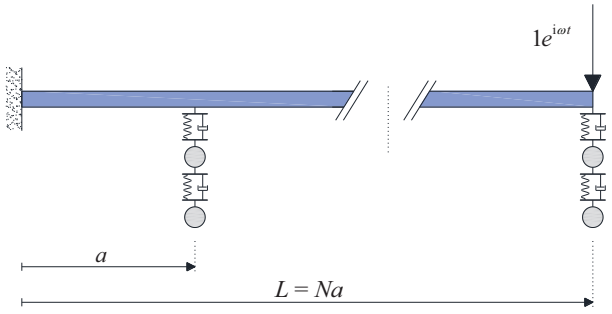

Fig. 10. Elastic LR beam with resonators in Fig. 2b.

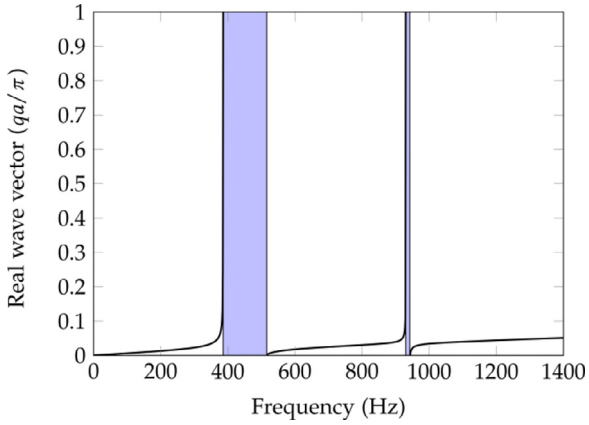

Fig. 11. Band gaps of the LR beam in Fig. 10.

4.2. Example B

Next, it is of interest to investigate the cantilever aluminium beam in Fig. 3 of Example A, when the laterally-resonant 2-DOF resonators in Fig. 2c are replaced with the 2-DOF resonators in Fig. 2b, as shown in Fig. 10.

The resonators in Fig. 10 are given the same mass/stiffness/damping properties of those in Fig. 3, with the aim of assessing whether and to which extent the different arrangement of masses/springs/dashpots within the two types of resonators may affect band gaps and dynamics of the beam. Therefore, following Example A, $N = 8$, $a = 0.02$ m, $m_1 = 0.01$ kg, $m_2 = 0.005$ kg, $k_1 = k_2 = 10^5$ Nm^{-1} and $c_1 = c_2 = 0.1$ Nsm^{-1} (see Fig. 2b).

For the infinite beam with no damping, Fig. 11 shows two band gaps in the frequency ranges 386–516 Hz and 930–942 Hz. It is apparent that the band gaps of the beam with resonators in Fig. 2b, see Fig. 11, are very different from those of the beam with resonators in Fig. 2c, see Fig. 4. Indeed, position as well as width of the band gaps change, demonstrating that various arrangements of masses/springs/dashpots may result in different elastic wave attenuation properties of the LR beam.

The proposed method is now applied to calculate transmittance and FRF of the cantilever beam in Fig. 10. Fig. 12 shows that, as expected, the transmittance is below 1 within the band gaps; however, values within the first band gap are significantly smaller than those within the second band gap and, in this respect, the behaviour of the beam in Fig. 10 proves quite different from the behaviour of the beam in Fig. 3.

Further, Fig. 13 demonstrates that the FRFs for the tip deflection under a harmonic load at the free end, as computed by the exact Eq. (18) and the approximate Eq. (36) using $M = 7$ modes, are in a perfect agreement (pertinent complex eigenvalues are in Table 2), confirming once again the accuracy of the proposed method.

Considering again Fig. 13, it is recognized that, within the band gaps, the FRF is generally well lower than the corresponding one of the beam without resonators. However, the FRFs of the beam with and without resonators are very close to each other at the right end of the second band gap. This behaviour appears similar to that of the beam in Fig. 3 but, in this case, is essentially attributable to the 3rd and 4th modes.

This conclusion is confirmed by Fig. 14 showing the time response of the beam to a unit sine force at the free end, with

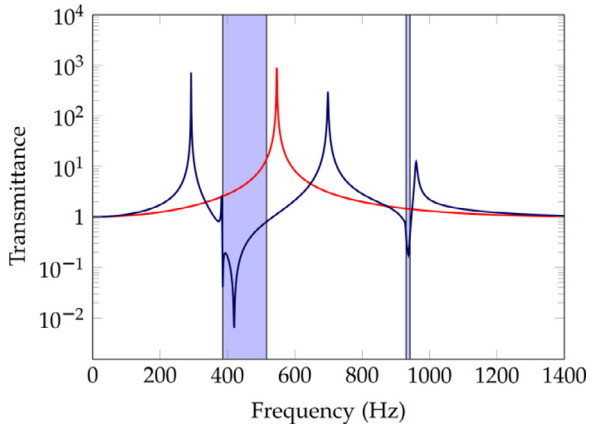

Fig. 12. Transmittance of the beam in Fig. 10: with resonators (blue) and without resonators (red). (For interpretation of the references to colour in this figure legend, the reader is referred to the web version of this article.)

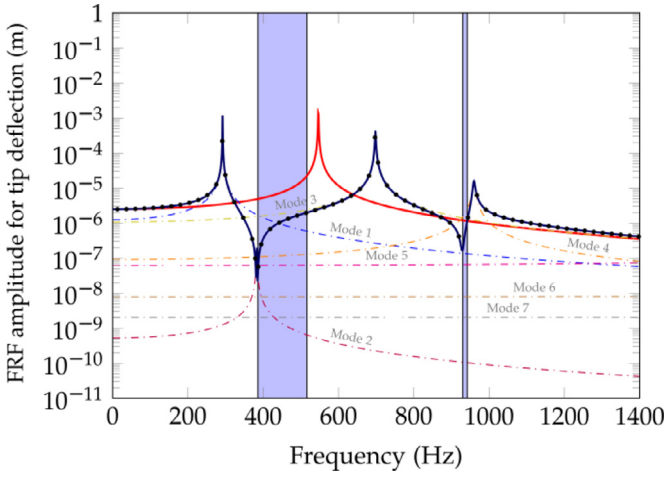

Fig. 13. FRF for the tip deflection of the beam in Fig. 10 under a unit harmonic force applied at the free end: Eq. (18) (blue); Eq. (36) with $M = 7$ modes (black dots); Eq. (34) for modal FRFs (color dashes); beam without resonators (red). (For interpretation of the references to colour in this figure legend, the reader is referred to the web version of this article.)

Table 2
Eigenvalues and damping ratios for modes of beam in Fig. 10.

Mode	Eigenvalue	Damping ratio
1	± 1835.184 + 0.822309i	0.000448
2	± 2404.434 + 2.852372i	0.001186
3	± 4386.564 + 5.289262i	0.001206
4	± 6029.053 + 17.46516i	0.002897
5	± 21,692.93 + 3.865147i	0.000178
6	± 60,314.17 + 3.808406i	0.000063
7	± 118,101.2 + 3.891800i	0.000033

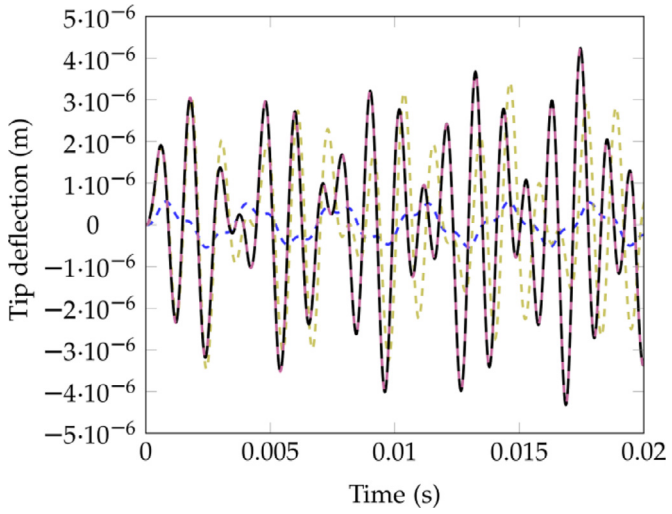

Fig. 14. Time response for the tip deflection of the beam in Fig. 10 under a 942-Hz unit sine force at the free end, for increasing number of modes M in Eq. (22): $M = 1$ (blue dashes), $M = 3$ (yellow dashes), $M = 5$ (pink dashes) $M = 7$ (black). (For interpretation of the references to colour in this figure legend, the reader is referred to the web version of this article.)

frequency equal to 942 Hz, i.e. the frequency at the right end of the second band gap. In accordance with the results in Fig. 13, the beam response is found to be mainly dominated by 3rd and 4th modal contributions, which cause the response of the beam with resonators (black line in Fig. 14) to attain the order of magnitude of the beam response without resonators (Fig. 9). In this case, therefore, the damping coefficients of the resonators should be appropriately selected so as to minimize the contribution of the 3rd and 4th modes. The conclusion is that the insight provided into the contribution of single modes to the beam response, in both frequency and time domain, is a most relevant advantage of the proposed method.

5. Conclusions

This paper has presented a comprehensive framework for the dynamic analysis of elastic LR infinite and finite beams. On demonstrating that the reaction force of a typical resonator depends on the deflection of the application point via a proper frequency-dependent stiffness, a transfer matrix method has been used to calculate the band gaps of the infinite beam, while for a finite beam the exact frequency response and exact modal responses have been derived in analytical form by a generalized function approach. The solutions hold for any number of resonators, proportional and non-proportional damping, providing a valuable tool to calculate the beam response to arbitrary loads and modal contributions for design purposes.

Declaration of Competing Interest

None.

Acknowledgments

Authors Giuseppe Failla, Roberta Santoro and Andrea Burlon gratefully acknowledge financial support from the Italian Ministry of Education, University and Research (MIUR) under the Prin 2017 grant “Multiscale Innovative Materials and Structures”.

Appendix

Following ref. [14], matrix $\mathbf{W}$ in Eq. (18) is given as (ω-dependence is omitted for brevity):

$$\mathbf{W}(x) = \mathbf{\Omega}(x) + \sum_{j=1}^{N} \mathbf{J}(x, x_j)\mathbf{\Phi}_{\mathbf{\Omega}}(x_j) + \sum_{j=2}^{N} \mathbf{J}(x, x_j) \sum_{2\le q\le j} \sum_{(j,m,n,\ldots,r,s)\in\mathbb{N}_q^{(j)}} \Phi_{\mathrm{J}}(x_j, x_m)\cdots\Phi_{\mathrm{J}}(x_r, x_s)\mathbf{\Phi}_{\mathbf{\Omega}}(x_s) \tag{A.1}$$

where $\mathbb{N}_q^{(j)}$ is the set including all possible q-ples of indexes (j, m, n, r, s) such that $j>m>n>r>s$, being $2 \le q \le j$.

In Eq. (A.1), $\mathbf{J}(x,x_j)$ is the 4×1 vector

$$\mathbf{J}(x, x_j) = \begin{Bmatrix} J_{V,P}(x, x_j) \\ J_{\Theta,P}(x, x_j) \\ J_{M,P}(x, x_j) \\ J_{S,P}(x, x_j) \end{Bmatrix} \tag{A.2}$$

while $\Phi_{\mathrm{J}}(x_j,x_k)$ denotes the scalar function $\Phi_{\mathrm{J}}(x_j,x_k) = -\kappa_j(\omega)J_{V,P}(x_j,x_k)$. Terms in $\mathbf{J}$ are derived using the beam equations

$$\frac{\mathrm{d}S(x)}{\mathrm{d}x} + \sum_{j=1}^{N} R_j\delta(x - x_j) + \rho\omega^2 V(x) = 0;\ \frac{\mathrm{d}M(x)}{\mathrm{d}x} = S(x) \tag{A.3a.b}$$

$$\frac{\mathrm{d}\Theta(x)}{\mathrm{d}x} = -\frac{M(x)}{EI};\ \frac{\mathrm{d}V(x)}{\mathrm{d}x} = \Theta(x) \tag{A.3c.d}$$

starting from the following particular integrals for deflection associated with a unit force at arbitrary $x = x_0$:

$$J_{V,P}(x, x_0) = \vartheta(\sinh(\beta(x - x_0)) - \sin(\beta(x - x_0)))H(x - x_0) \tag{A.4}$$

where $\vartheta = \vartheta(\omega) = 2^{-1}(EI)^{-1/4}\rho^{-3/4}\omega^{-3/2}$ and $\beta = \beta(\omega) = (EI)^{-1/4}\rho^{1/4}\omega^{1/2}$. Again in Eq. (A.1), $\mathbf{\Omega}(x)$ depends on the solution to the homogeneous equation associated with Eq. (16), i.e.

$$\mathbf{\Omega}(x) = \begin{bmatrix} \mathrm{e}^{-\beta x} & \mathrm{e}^{\beta x} & \cos(\beta x) & \sin(\beta x) \\ -\beta\mathrm{e}^{-\beta x} & \beta\mathrm{e}^{\beta x} & -\beta\sin(\beta x) & \beta\cos(\beta x) \\ -EI\beta^2\mathrm{e}^{-\beta x} & -EI\beta^2\mathrm{e}^{\beta x} & EI\beta^2\cos(\beta x) & EI\beta^2\sin(\beta x) \\ EI\beta^3\mathrm{e}^{-\beta x} & -EI\beta^3\mathrm{e}^{\beta x} & -EI\beta^3\sin(\beta x) & EI\beta^3\cos(\beta x) \end{bmatrix} \tag{A.5}$$

while $\mathbf{\Phi}_{\mathbf{\Omega}}(x_s)$ in Eq. (A.1) is the row vector $\mathbf{\Phi}_{\mathbf{\Omega}}(x_s) = -\kappa_j(\omega)\{(\mathbf{\Omega}(x_s))_1\}$, with $()_l$ indicating the lth row of the matrix within parenthesis.

Finally, in Eq. (18) vector $\mathbf{Y}^{(f)}(x)$ is given as (again ω-dependence is omitted for brevity)

$$\mathbf{Y}^{(f)}(x) = \mathbf{F}(x) + \sum_{j=1}^{N} \mathbf{J}(x, x_j)\Phi^{(f)}(x_j) + \sum_{j=2}^{N} \mathbf{J}(x, x_j) \sum_{2\le q\le j} \sum_{(j,m,n,\ldots,r,s)\in\mathbb{N}_q^{(j)}} \Phi_{\mathrm{J}}(x_j, x_m)\cdots\Phi_{\mathrm{J}}(x_r, x_s)\Phi^{(f)}(x_s) \tag{A.6}$$

where $\Phi^{(f)}(x_s)$ is the scalar function $\Phi^{(f)}(x_s) = -\kappa_j(\omega)F_1(x)$, with F_1 denoting the 1st component of vector

$$\mathbf{F}(x) = \int_0^L \mathbf{J}(x, y)f(y)dy \tag{A.7}$$

References

[1] Y. Xiao, J. Wen, X. Wen, Broadband locally resonant beams containing multiple periodic arrays of attached resonators, Phys. Lett. A 376 (2012) 1384–1390.

[2] J.S. Chen, B. Sharma, C.T. Sun, Dynamic behavior of sandwich structure containing spring-mass resonators, Compos. Struct. 93 (2011) 2120–2125.
[3] Y. Xiao, J. Wen, D. Yu, X. Wen, Flexural wave propagation in beams with periodically attached vibration absorbers: band-gap behavior and band formation mechanisms, J. Sound Vib. 332 (2013) 867–893.
[4] Y. Xiao, J. Wen, G. Wang, X. Wen, Theoretical and experimental study of locally resonant and Bragg band gaps in flexural beams carrying periodic arrays of beam-like resonators, J. Vib. Acoust. 135 (2013) 041006.
[5] H. Sun, X. Du, P.F. Pai, Theory of metamaterial beams for broadband vibration absorption, J. Intell. Mater. Syst. Struct. 21 (2010) 1085–1101.
[6] R. Zhu, X.N. Liu, G.K. Hu, C.T. Sun, G.L. Huang, A chiral elastic metamaterial beam for broadband vibration suppression, J. Sound. Vib. 333 (2014) 2759–2773.
[7] P.F. Pai, Metamaterial-based broadband elastic wave absorber, J. Intell. Mater. Syst. Struct. 21 (2010) 517–528.
[8] G. Hu, L. Tang, R. Das, Internally coupled metamaterial beam for simultaneous vibration suppression and low frequency energy harvesting, J Appl. Phys. 123 (2018) 055107.
[9] A. Casalotti, S. El-Borgi, W. Lacarbonara, Metamaterial beam with embedded nonlinear vibration absorbers, Int J. Non. Linear Mech. 98 (2018) 32–42.
[10] T. Wang, M.-P. Sheng, Q.-H. Qin, Multi-flexural band gaps in an Euler–Bernoulli beam with lateral local resonators, Phys. Lett. A 380 (2016) 525–529.
[11] F. Romeo, A. Luongo, Invariant representation of propagation properties for bi–coupled periodic structures, J. Sound Vib. 257 (2002) 869–886.
[12] D. Yu, Y. Liu, G. Wang, H. Zhao, J. Qiu, Flexural vibration band gaps in Timoshenko beams with locally resonant structures, J. Appl. Phys. 100 (12) (2006) 124901.
[13] G. Failla, M. Di Paola, A. Pirrotta, A. Burlon, I. Dunn, Random vibration mitigation of beams via tuned mass dampers with spring inertia effects, Meccanica 54 (9) (2019) 1365–1383.
[14] G. Failla, An exact modal analysis approach to vibration analysis of structures with mass-spring subsystems and rotational joints, J. Sound. Vib. 438 (2019) 191–219.
[15] G. Failla, An exact generalised function approach to frequency response analysis of beams and plane frames with the inclusion of viscoelastic damping, J. Sound. Vib. 360 (2016) 171–202.
[16] G. Falsone, The use of generalised functions in the discontinuous beam bending differential equation, Int. J. Eng. Educ. 18 (3) (2002) 337–343.
[17] S. Caddemi, I. Caliò, The exact explicit dynamic stiffness matrix of multi--cracked Euler–Bernoulli beam and applications to damaged frame structures, J. Sound Vib. 332 (12) (2013) 3049–3063.
[18] J. Wang, P. Qiao, Vibration of beams with arbitrary discontinuities and boundary conditions, J. Sound Vib. 308 (2007) 12–27.
[19] A. Yavari, S. Sarkani, E.T. Moyer, On applications of generalized functions to beam bending problems, Int. J. Solids Struct. 37 (2000) 5675–5705.
[20] A. Burlon, G. Failla, F. Arena, Exact frequency response analysis of axially loaded beams with viscoelastic dampers, Int. J. Mech. Sci. 115-116 (2016) 370–384.
[21] Y. Liu, D. Yu, L. Li, H. Zhao, J. Wen, X. Wen, Design guidelines for flexural wave attenuation of slender beams with local resonators, Phys. Lett. A 362 (2007) 344–347.
[22] Y. Gao, M.J. Brennan, F. Sui, Control of flexural waves on a beam using distributed vibration neutralisers, J. Sound Vib. 330 (2011) 2758–2771.